Fun With TBN
Ver. 1

S. Ellingson*

September 13, 2011

Contents

*Virginia Tech. E-mail: `ellingson@vt.edu`.

1   Introduction

This memo demonstrates the use of 74.03 MHz TBN data for array calibration and beamforming in observations of the strong radio sources Cas A and Cyg A. Specifically:

- The calculation of phase-and-sum beamforming coefficients directly from TBN observations of Cyg A is demonstrated. Said differently, it is possible to "phase up" the array on Cyg A having only TBN output and no information about array geometry or instrumental phases. (This is henceforth referred to as "blind" beamforming.)

- Using just one set of "known good" beamforming coefficients (namely, those obtained above) plus the array geometry, the beam can be accurately pointed in other directions. In particular, it is demonstrated that it is possible to point a beam at Cas A using only the Cyg A beamforming coefficients and the array geometry.

- The beam sensitivity – specifically, system equivalent flux density (SEFD) – is extracted from observations of Cyg A, and is found to be 8.68 kJy for this pointing using 1 polarization. Scaling this value to account for both polarizations and assuming all dipoles working, the SEFD is 4.05 kJy. This is about 20% better than the value predicted for the same zenith angle in LWA Memo 166.[1]

- The known ratio of the flux densities of Cas A to Cyg A was used to estimate the ratio of the power patterns of the dipoles in the directions of these two sources. The results were distributed over a 3.8 dB range (1σ). However, the mean value is within $\sim 20\%$ of the ratio predicted using the "standalone stand" model of LWA Memo 175, and the variation is consistent with the mutual coupling-induced variations predicted in LWA Memo 166.

A few concerns that merit future attention are also noted. These include:

- The peak sidelobe levels of the phase-and-sum beam appear to be about -10 dB – much higher than expected from previous studies. It is possible that this is due to mutual coupling.

- A large irregular oscillation on time scales of 10–100 s is seen in the beamformer output. The same oscillation appears to be present in the individual baselines (although it is hard to be sure about this). Possible causes include ionospheric scintillation and locally-generated multipath.

- The "DC" term in the dipole-to-outrigger fringes seems much larger than the sum of the expected contributions (namely, the "DC" term of the sky brightness correlation, and crosstalk within the instrument).

2   Description of the Data

All work described in this memo is from the single dataset `055792_001156533`, which is 60 minutes of 100 kSPS TBN data starting at 22:12 MDT August 18, 2011. The instantaneous bandwidth of this data is approximately $B = 67$ kHz. At the mid-point of this observation (22:42 MDT), the positions of Cyg A and Cas A were as indicated in Table 1.

LWA-1 appears to have been in good working order during the data collection, although 21 of 260 stands were excluded from analysis either because they are not installed (e.g., stands 257, 259, and 260), exhibited low signal level, or exhibited some other anamoly (e.g. failed to produce the expected fringes). Thus, a total of 239 stands are used in the analyses described in this memo. Only the North-South-aligned polarizations of these stands are used, so a total of 239 dipoles are considered.

---

[1]It should be noted that SEFD depends on both pointing relative to the zenith (due to beam gain) as well as pointing with respect to RA/Dec (due to externally-dominated system temperature).

Source	RA (h:m:s)	Dec (d:m:s)	Az (d:m:s)	Z (d:m:s)	Flux density
Cyg A	19:59:28.35	+40:44:02.1	46:07:35	10:11:14	17.06 kJy
Cas A	23:23:26.00	+58:48:00.0	38:29:11	46:26:32	17.13 kJy

Table 1: Astronomical source data relevant to this dataset. Azimuth and zenith angle (Z) are specified for the midpoint time of the observation. The flux densities are the 73.8 MHz values given in LWA Memo 155 [1], scaled to 74.03 MHz using $\alpha = -0.58$ and $\alpha = -0.72$ for Cyg A and Cas A respectively, and Cas A is further scaled by -0.75%/yr [2].

The data are output from LWA1 in complex-valued baseband "I-Q" format, with 8 bits for I and 8 bits for Q. A frequency of zero in this dataset corresponds to a sky frequency of 74.03 MHz. RFI conditions appear to have been relatively benign, as is apparent in the results presented in this memo. As part of (my) standard RFI mitigation procedures, about 0.03% of the samples (those having the largest magnitudes) were "plinked"; i.e., set to zero. The plinked samples are roughly uniformly distributed throughout the dataset; i.e., generally not associated with long (i.e., many contiguous samples) events.

3   Theory and Assumptions

The analyses described in this memo are entirely narrowband; that is, it is assumed that delays are perfectly represented as phase shifts. This is justified by the fact that that the maximum time-of-flight across the longest baseline in the array (about 390 m) is 1.3 μs $<<$ the sample period $(100 \text{ kSPS})^{-1} = 10$ μs. Within the station array itself – i.e., excluding the "outrigger" stand (258) – the maximum time-of-flight decreases to about 0.4 μs. Lifting the narrowband assumption (either by channelizing the data and operating on narrower subbands, or by using fractional sample delay techniques in lieu of phase-only processing) might yield slightly better results, but probably not significant improvement in the context of this study.

For later convenience, we now introduce some mathematical shorthand. The voltage induced at dipole n is assumed to have the form

$$u_n(t) = a_n(\psi_1)s_1(t) + a_n(\psi_2)s_2(t) + z_n(t) \tag{1}$$

where $s_1(t)$ and $s_2(t)$ are the signals incident from discrete point sources 1 and 2 at a reference point at the origin of the array coordinate system, $a_n(\psi)$ represents the response of antenna n to a signal incident from direction ψ (including the effect of displacement from the origin), and $z_n(t)$ is the signal induced in antenna n by external noise. "ψ" is shorthand for a two-dimensional pointing (e.g., θ & ϕ, or altitude & azimuth). External noise is assumed to dominate over internal noise, although this assumption will not prove to be important in subsequent analysis here.

The value which is actually measured, $x_n(t)$, depends on the instrumental gain and phase c_n (a complex coefficient), which is assumed to be time invariant, so that $x_n(t) = c_n u_n(t)$. For convenience, we define $h_n(\psi) = c_n a_n(\psi)$ so that

$$x_n(t) = h_n(\psi_1)s_1(t) + h_n(\psi_2)s_2(t) + c_n z_n(t) \ . \tag{2}$$

Let $y(\psi_p, t)$ be the output of the phase-and-sum beamformer which points in direction ψ_p, where $p = 1$ (for source 1) or 2 (for source 2). This output can be written in the form

$$y(\psi_p, t) = \sum_{n=1}^{N} b_n(\psi_p)x_n(t) \ , \tag{3}$$

where the phase-and-sum beamforming coefficients $b_n(\psi_p)$ are given by

$$b_n(\psi_p) = \frac{h_n^*(\psi_p)}{|h_n(\psi_p)|} \ . \tag{4}$$

This leaves the question of how to determine the $h_n(\psi_p)$'s. One possible strategy is simply to use the definition $h_n(\psi_p) = c_n a_n(\psi_p)$, which would require accurate knowledge of the array geometry (currently reasonable to assume), accurate knowledge of the antenna patterns (*not* safe to assume) and accurate knowledge of the instrumental gains and phases (currently not safe to assume in light of recently discovered DP issues). Alternatively, we can obtain the $h_n(\psi_p)$'s (and subsequently the $b_n(\psi_p)$'s) directly from the data. The procedure is derived below.

The correlation between the data $x_n(t)$ and $x_m(t)$ collected from any two antennas n and m is

$$\rho_{nm}(t) = \int_{t-\tau}^{t} x_n(t')x_m^*(t')dt' = \langle x_n(t)x_m^*(t)\rangle \tag{5}$$

where τ is the integration time, and the "angle brackets" notation on the right is used as a convenient shorthand for time domain averaging. Assuming the $x_n(t)$'s have the form of Equation 2, and assuming $s_1(t)$, $s_2(t)$, and the $z_n(t)$'s are mutually uncorrelated, ρ_{nm} has the form

$$\rho_{nm}(t) = h_n(\psi_1)h_m^*(\psi_1)\left\langle |s_1(t)|^2 \right\rangle + h_n(\psi_2)h_m^*(\psi_2)\left\langle |s_2(t)|^2 \right\rangle + c_n c_m^* \left\langle z_n(t)z_m^*(t)\right\rangle \ . \tag{6}$$

Let $S_1 = \left\langle |s_1(t)|^2 \right\rangle$, and note S_1 is time-invariant if the flux of source 1 is time-invariant. Similarly, $S_2 = \left\langle |s_2(t)|^2 \right\rangle$. Employing this notation, we have

$$\rho_{nm}(t) = h_n(\psi_1)h_m^*(\psi_1)S_1 + h_n(\psi_2)h_m^*(\psi_2)S_2 + c_n c_m^* \left\langle z_n(t)z_m^*(t)\right\rangle \ . \tag{7}$$

It will be demonstrated in the next section that it is possible to identify and separate the three terms in the above equation when $\rho_{nm}(t)$ is obtained directly from data. Let the first term – the part of the correlation associated with the source 1 – be $\rho_{nm}^{(1)}(t)$; i.e.,

$$\rho_{nm}^{(1)}(t) = h_n(\psi_1)h_m^*(\psi_1)S_1 \ . \tag{8}$$

Now, imagine we obtain $\rho_{nm}^{(1)}(t)$ for $n = 1...N$ and some fixed m (we will choose m to correspond to the outrigger dipole later, but this is not important at the moment), from the data, using Equation 5. From this set of N correlations, let us choose just one – we shall call it $\rho_{lm}^{(1)}(t)$ – to be a "reference" correlation. Now note for each n:

$$\frac{\rho_{nm}^{(1)}(t)}{\rho_{lm}^{(1)}(t)} = \frac{h_n(\psi_1)h_m^*(\psi_1)S_1}{h_l(\psi_1)h_m^*(\psi_1)S_1} = \frac{h_n(\psi_1)}{h_l(\psi_1)} \ . \tag{9}$$

Further, note

$$\left[\frac{\rho_{nm}^{(1)}(t)}{\rho_{lm}^{(1)}(t)}\right]^* \left|\frac{\rho_{nm}^{(1)}(t)}{\rho_{lm}^{(1)}(t)}\right|^{-1} = \left(\frac{h_n(\psi_1)}{h_l(\psi_1)}\right)^* \left|\frac{h_n(\psi_1)}{h_l(\psi_1)}\right|^{-1} = \frac{h_n^*(\psi_1)}{|h_n(\psi_1)|}\left[\frac{h_l^*(\psi_1)}{|h_l(\psi_1)|}\right]^{-1} = b_n(\psi_1)\left[\frac{h_l^*(\psi_1)}{|h_l(\psi_1)|}\right]^{-1} \ . \tag{10}$$

In other words: the above N values, which can be obtained from data, give us the N phase-and-sum beamforming coefficients times a unity-magnitude constant which is the same for all n. Since the only difference from $b_n(\psi_1)$ is a phase shift which is the same for all n, these values are equally suitable as phase-and-sum beamforming coefficients. We shall refer to the coefficients obtained in this way as the $b_n^{(l)}(\psi_1)$'s. Similarly, we may obtain $b_n^{(l)}(\psi_2)$'s, which are the beamforming coefficients for pointing toward ψ_2 (source 2).

Summarizing: The "blind" procedure for generating the N phase-and-sum beamforming coefficients $b_n^{(l)}(\psi_p)$ is as follows:

4

1. Obtain the N correlations $\rho_{nm}(t)$ with respect to antenna m (we will use the outrigger dipole) using Equation 5;

2. Extract the $\rho_{nm}^{(p)}(t)$'s (contributions to $\rho_{nm}(t)$'s from the source of interest) using the method described in the next section; and then

3. Divide each $\rho_{nm}^{(p)}(t)$ by one of the correlations ($\rho_{lm}^{(p)}(t)$), conjugate, and divide by the magnitude, as shown in Equation 10.

It should be noted that this procedure makes no assumptions about mutual coupling or the uniformity of antenna patterns; thus the best possible result will be obtained regardless of the effects of mutual coupling and independently of the details of the antenna pattern.

Finally, we consider the problem of how to point a beam in directions other than ψ_1 or ψ_2; i.e., directions other than those for which we have strong point sources available for blind calibration. From Equation 9, we have

$$\frac{\rho_{nm}^{(1)}(t)}{\rho_{lm}^{(1)}(t)} = \frac{h_n(\psi_1)}{h_l(\psi_1)} = \frac{c_n a_n(\psi_1)}{h_l(\psi_1)} \ . \tag{11}$$

We define $c_n^{(l)}$ as follows:

$$c_n^{(l)} = \left[\frac{\rho_{nm}^{(1)}(t)}{\rho_{lm}^{(1)}(t)} \right] a_n^{-1}(\psi_1) = \frac{c_n}{h_l(\psi_1)} \ . \tag{12}$$

Note that the $c_n^{(l)}$'s are simply the c_n's times a constant which is the same for all n. Now from Equation 4:

$$b_n(\psi_1) = \frac{h_n^*(\psi_1)}{|h_n(\psi_1)|} = \frac{c_n^* a_n^*(\psi_1)}{|c_n a_n(\psi_1)|} = \frac{\left(c_n^{(l)}\right)^* a_n^*(\psi_1)}{\left|c_n^{(l)} a_n(\psi_1)\right|} \frac{h_l^*(\psi_1)}{|h_l(\psi_1)|} \ . \tag{13}$$

Now from Equation 10 we have:

$$b_n^{(l)}(\psi_1) = \frac{\left(c_n^{(l)}\right)^* a_n^*(\psi_1)}{\left|c_n^{(l)} a_n(\psi_1)\right|} \ . \tag{14}$$

Thus, the $c_n^{(l)}$'s can be determined directly from data if the $a_n(\psi_1)$'s are known. Then, the corresponding phase-and-sum beamforming coefficients for any other direction ψ are obtained using the same $c_n^{(l)}$'s with the appropriate $a_n(\psi)$'s, as follows:

$$b_n^{(l)}(\psi) = \frac{\left(c_n^{(l)}\right)^* a_n^*(\psi)}{\left|c_n^{(l)} a_n(\psi)\right|} \ . \tag{15}$$

Summarizing: The "repointing without recalibrating" procedure for generating phase-and-sum beamforming coefficients for any direction ψ is as follows:

1. Obtain the $\rho_{nm}^{(p)}(t)$'s from the data, using steps 1 and 2 of the "blind" procedure described earlier, using any strong point source p.

2. Compute the $c_n^{(l)}$'s using Equation 12.

3. Compute the $b_n^{(l)}(\psi)$'s using Equation 15.

Note that above procedure assumes knowledge of the $a_n(\psi)$'s. These are not known accurately (although for the special cases of $a_n(\psi_1)$ and $a_n(\psi_1)$ they can be extracted from data; and perhaps for other ψ they could be determined using electromagnetic modeling). In this memo, we demonstrate

that it is possible to form a beam in the desired direction by assuming that the $a_n(\psi)$'s are determined solely by array geometry – i.e., the geometry-induced phase shifts due to antenna positions – neglecting the antenna patterns and any differences in the antennas patterns due to mutual coupling or other considerations.

4 Analysis of the Correlations

The phase-and-sum beamforming procedure described above depends on finding $\rho_{nm}^{(p)}(t)$; i.e., the contribution of source p ($p = 1$ or 2) to the correlations $\rho_{nm}(t)$ between each antenna n and the reference antenna m. We now tackle this aspect of the problem.

The observed correlation $\rho_{nm}(t)$ when n is Stand 248 (located on the far west side of the station array) and m is Stand 258 (the outrigger) is shown in Figures 1 and 2. In these figures and throughout this memo, the integration time $\tau = 10$ s. A fringe pattern is clearly visible with high signal-to-noise ratio.

Figure 3 shows the Fourier transform of the fringe pattern shown in Figures 1 (and 2). To mitigate endpoint effects, a triangular window has been applied to the data before the Fourier transform and the data has been scaled by a factor of 2 to compensate. The transform reveals that the result is strongly dominated by three clearly-identifiable components: From left to right, these are Cyg A (50% of the power), Cas A (21%), and a zero-frequency ("DC") term (about 16%). The associations with Cyg A and Cas A can be confirmed from their fringe rates, which depend only on the length and orientation of the baseline. The "DC" term is a combination of a number of contributions, including the "DC" term in the spatial correlation of the sky brightness temperature (see Figure 13 of [3]) and crosstalk internal to the instrument. However, the observed DC component is quite large compared to the sum of these expected contributions, and should be more carefully studied. For the purposes of this memo, however, it is important only that we be able to separate it from the the contributions of Cyg A and Cas A. In any event, Figure 3 confirms the validity of the two-source-plus-noise model proposed in Section 3, at least for this particular dataset.

Because the contributions of Cyg A and Cas A are well-separated in fringe rate from each other and from the DC term, it is straightforward to separate them. In this study, we simply set to zero all samples outside the expected range of fringe rates for the desired source p in the Fourier transform of the correlation, and then take the inverse Fourier transform. The result is $\rho_{nm}^{(p)}(t)$, plus a tiny residual which is not associated with source p, but just happens to fall within the same range of fringe rates. It should be noted that this method is not completely foolproof, as it is conceivable that the fringe rates associated with some baselines may be too close to separate. This was not carefully checked, however it does not appear to be have been a significant problem in this dataset/study.

Before moving on, it is interesting to note that Figure 3 already provides sufficient information to estimate the relative gains between two points in the antenna pattern; namely those corresponding to the directions to Cyg A and Cas A. Since the known Cas A / Cyg A flux ratio is currently within $\sim 1\%$ of 1, the ratios of the corresponding peaks in Figure 3 is essentially the gain ratio. Here it is $0.42 = -3.7$ dB. For comparison, we can obtain this also by using the "standalone stand" model described in LWA Memo 175 [4] (see also [5]); this model predicts -2.8 dB, for an "error" of -0.9 dB. Figure 7 of LWA Memo 166 [3] suggest that mutual coupling could change the latter result by roughly ± 2 dB, so the difference could be attributable to mutual coupling. To get a better idea, this experiment was repeated for all 239 dipole-outrigger baselines; the mean was found to be 0.62 with a standard deviation $\sigma = 0.26$. The corresponding mean$-\sigma$, mean, and mean$+\sigma$ values are -4.3, -2.1, and -0.6 dB, respectively. The corresponding "errors" relative to the model prediction are -1.6, $+0.7$, and $+2.2$ dB. Thus, it seems that the model fits the data fairly well in an average
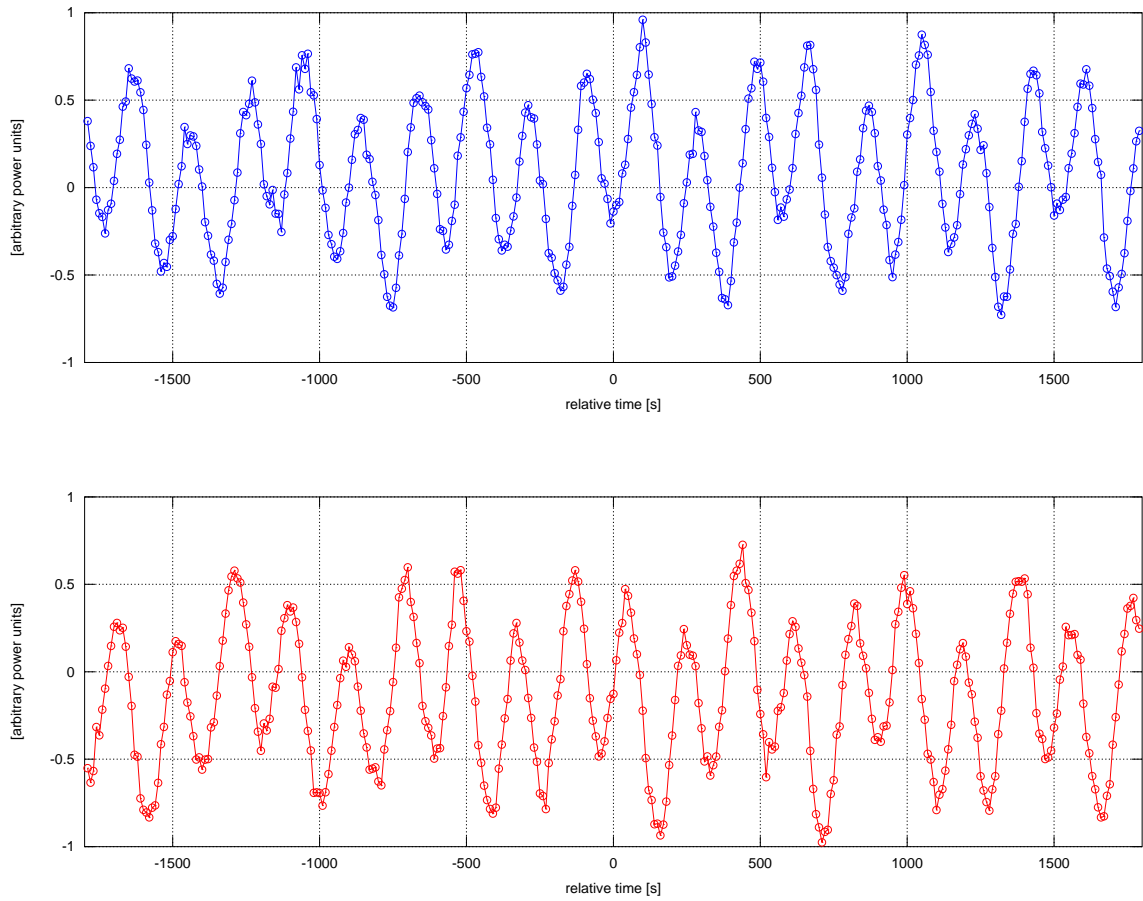
Figure 1: $\rho_{nm}(t)$, where n is Stand 258 and m is the outrigger. *Top*: Real part; *Bottom*: Imaginary part.
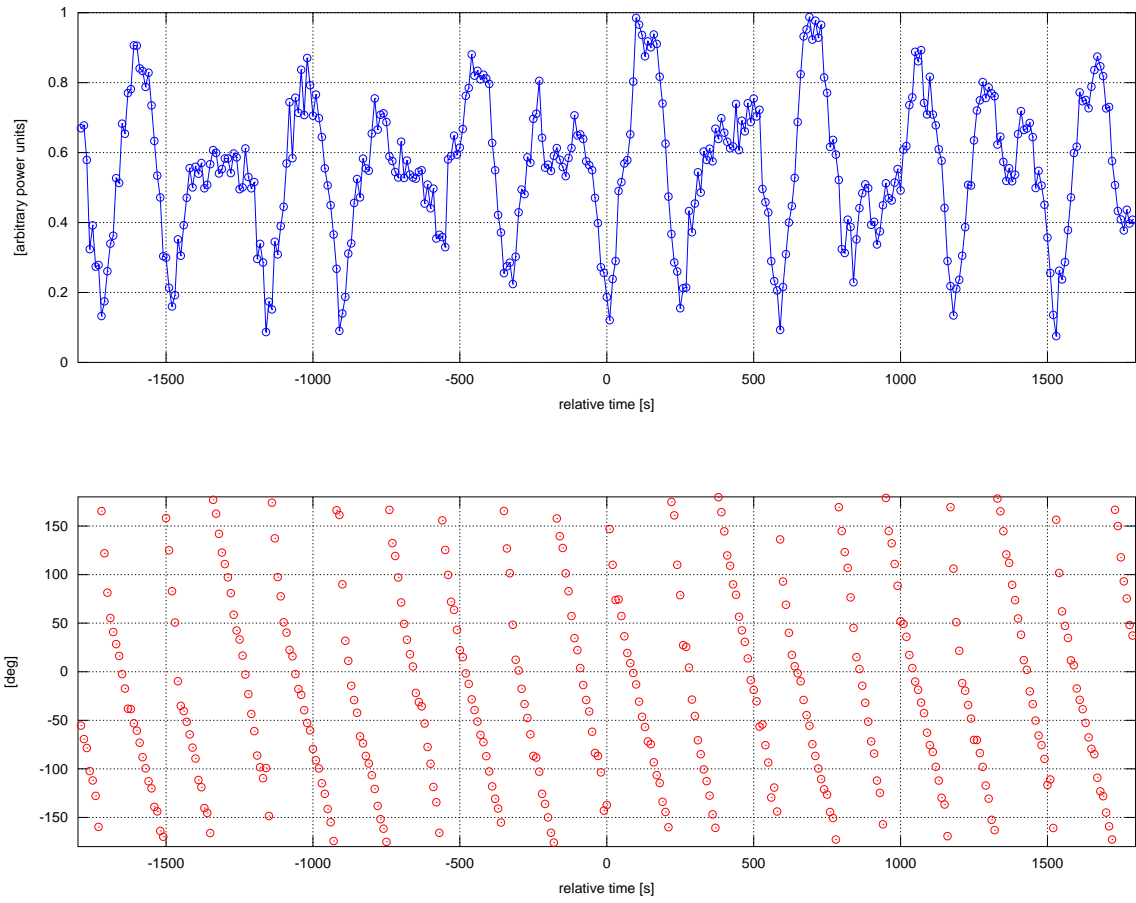
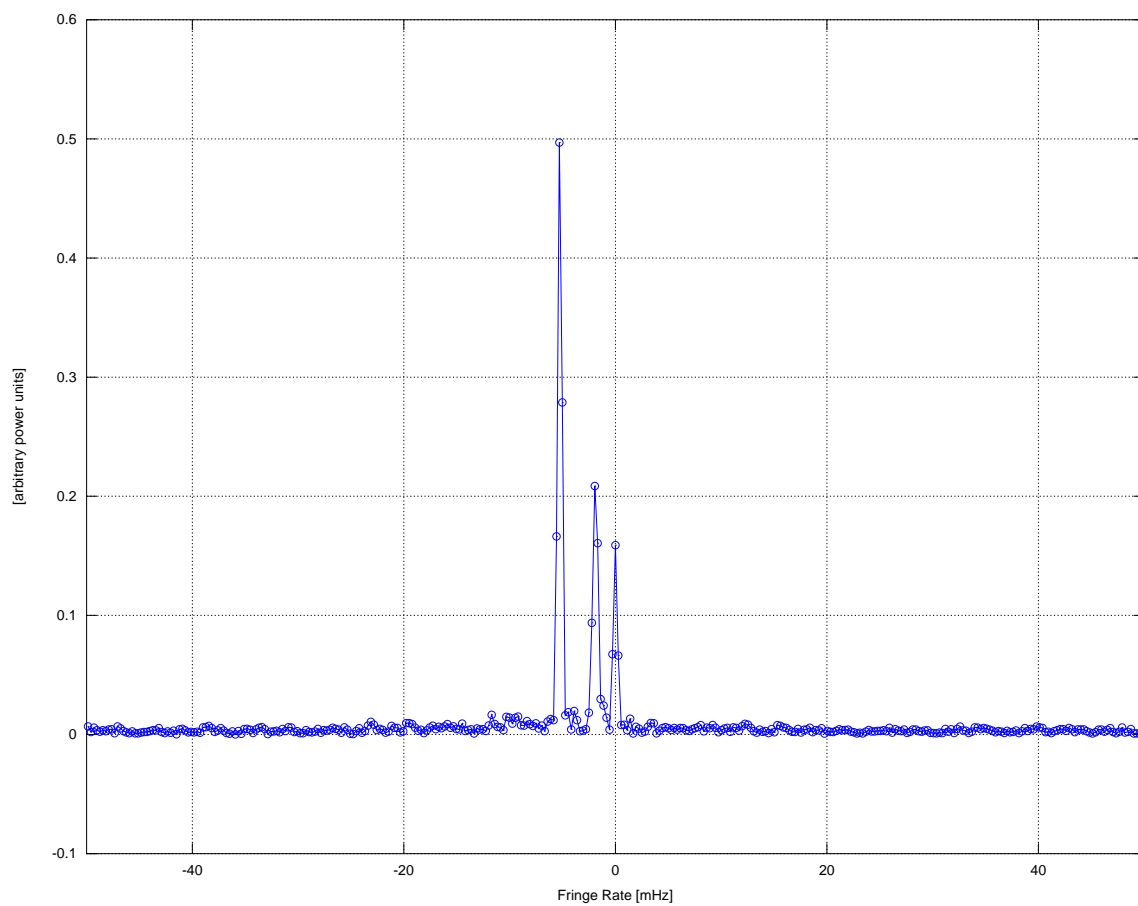Figure 2: Same as Figure 1, except now the top plot is magnitude, and the bottom plot is phase.

8

Figure 3: Magnitude of the Fourier transform of the fringe pattern shown in Figure 1. The resolution is 279 μHz.

sense, but the results are highly variable from baseline to baseline. This is presumably due to mutual coupling, as the observed range of variation is roughly as predicted by Figure 7 of LWA Memo 166.

5 "Blind" Beamforming

We now demonstrate the "blind" beamforming procedure described in Section 3. Beamforming coefficients are obtained for Cyg A ("$p = 1$") at the midpoint of the dataset. These coefficients then define a fixed beam through which Cyg A drifts. The result is shown in Figure 4.

From this result and the known flux density of Cyg A (see Table 1) it is possible to estimate the sensitivity of the beam; specifically, the system equivalent flux density (SEFD) for this source and pointing. The SEFD is simply the known flux density divided by the apparent signal-to-noise ratio (SNR). The SNR can be estimated as peak power P_{on} minus the estimated non-source-related power P_{off}, divided by P_{off}. From Figure 4, $P_{on} \approx 6.70$, $P_{off} \approx 2.26$ (extrapolating across the apparent noise baseline), and so the SEFD is estimated to be 8.68 kJy.

Because LWA1 is strongly sky-noise dominated, a large fraction of the system temperature is due to sky noise received through the main lobe and sidelobes of the beam. This makes it difficult to accurately determine the shape of the beam from Figure 4. The contribution due to distributed sources (e.g., the all-sky "DC" contribution, the Galactic plane, etc.) can be dramatically reduced by correlating the beamformer output with the outrigger dipole. The result in this case is shown in Figure 5. The beamwidth is approximately as expected, with FWHM$\approx 4°$. Note the first sidelobes are clearly visible. The first sidelobe level appears to be approximately -10 dB, which is much higher than predicted in analyses used to design the array geometry [6]. A second concern is the large, rapid oscillation observed across the main lobe of the beam. It is possible that this is ionospheric scintillation; this is considered further in Section 7.

The process is repeated to produce a beam which points at Cas A ("$p = 2$") at the midpoint of the dataset. These coefficients then define a fixed beam through which Cas A drifts. The result is shown in Figure 6. Note that the beam is significantly wider; however this is expected as Cas A is at $Z \approx 46°$ whereas Cyg A is at $Z \approx 10°$. The same type of oscillations noted in the Cyg A beam are again clearly visible.

6 Repointing Without Recalibrating

We now demonstrate the "repointing without recalibrating" (henceforth: "RWR") beamforming procedure described in Section 3. Instrumental gains and phases ($c_n^{(l)}$'s) are obtained using Cyg A at the midpoint of the dataset. The a_n's are obtained from array geometry (only) and pointing direction, assuming (implicitly) that the antennas are isotropic and identical. We then attempt repointing to:

- The position of Cyg A 15 minutes prior to the midpoint of the dataset (Figure 7),

- A position $10°$ toward the horizon relative to the position of Cyg A at the midpoint of the dataset (Figure 8), and

- Cas A (Figure 9).

Note that in each case we obtain the expected result. However, careful comparison of Figures 6 (blind beamforming on Cas A) and 9 (RWR beamforming on Cas A after calibrating on Cyg A) indicates that the beams are not identical.
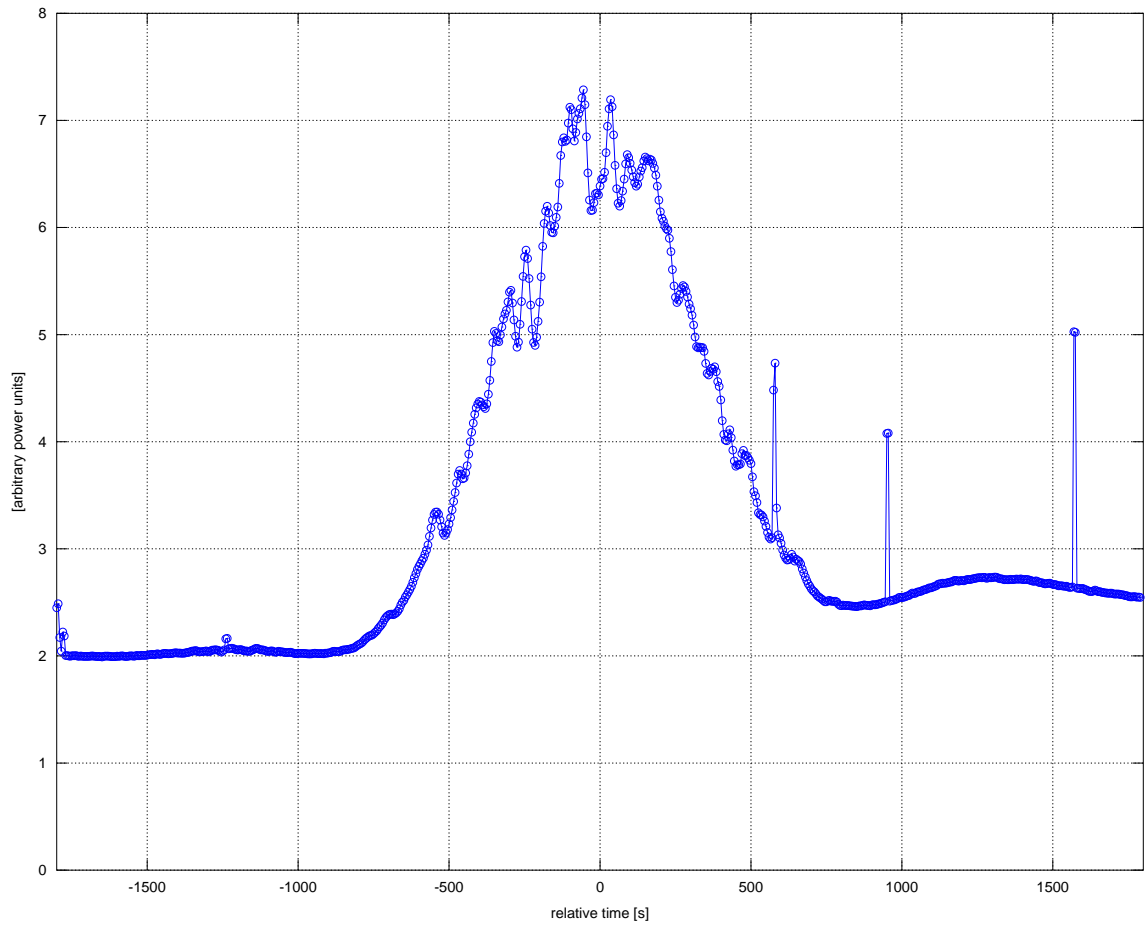
Figure 4: "Blind" beamforming: Cyg A drift scan. The three spikes in the last half of the plot are apparently RFI.
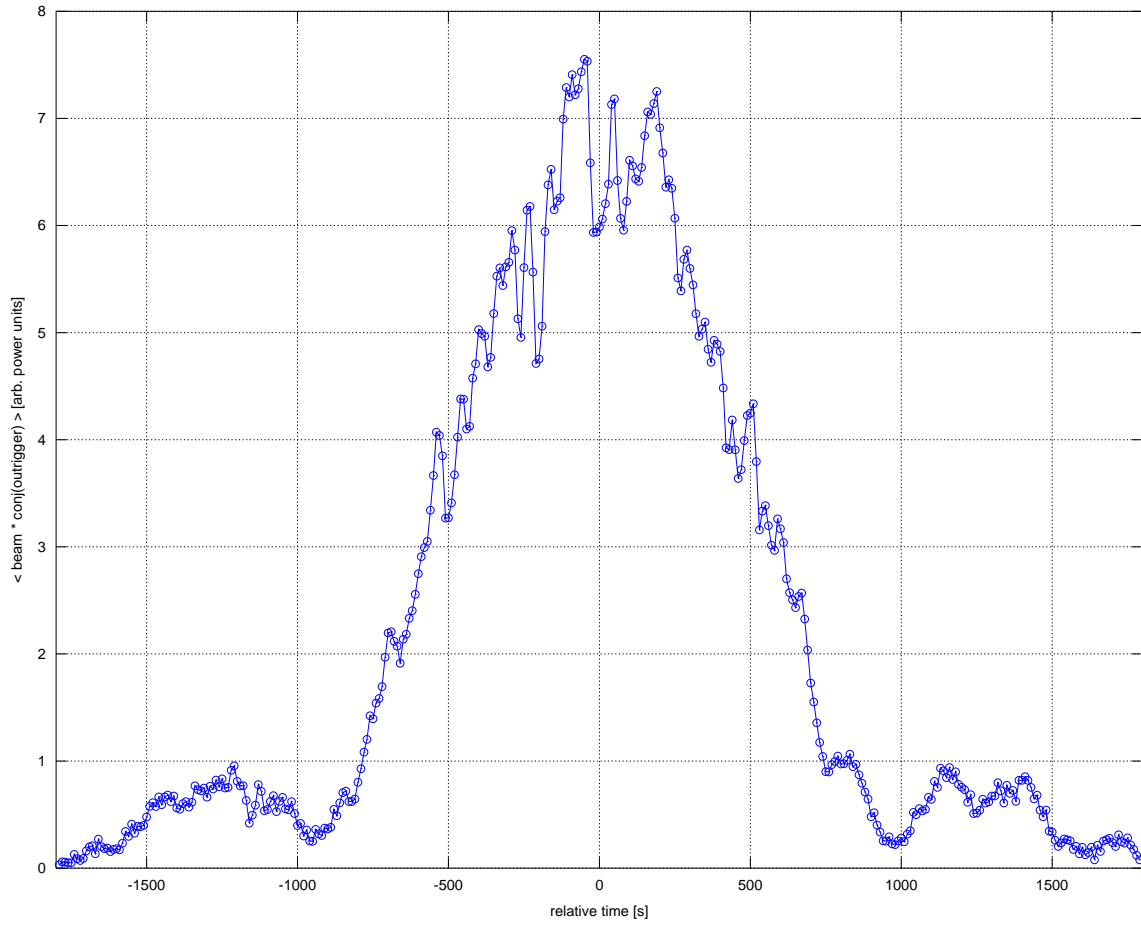
Figure 5: "Blind" beamforming: Same as Figure 5, except now the Cyg A beam is correlated against the outrigger dipole.
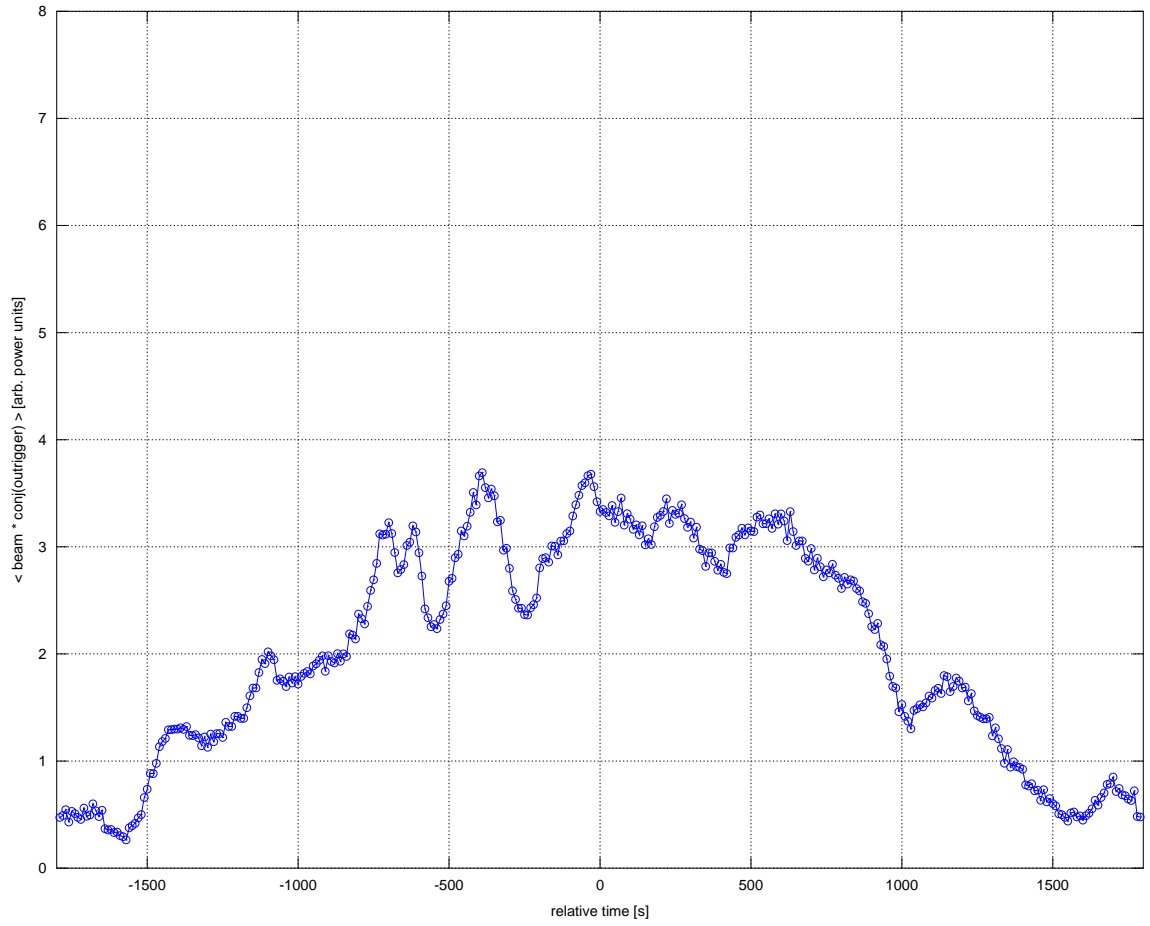
Figure 6: "Blind" beamforming: Same as Figure 5, except now the beam is phased up on Cas A at the midpoint of the dataset, and correlated against the outrigger dipole.
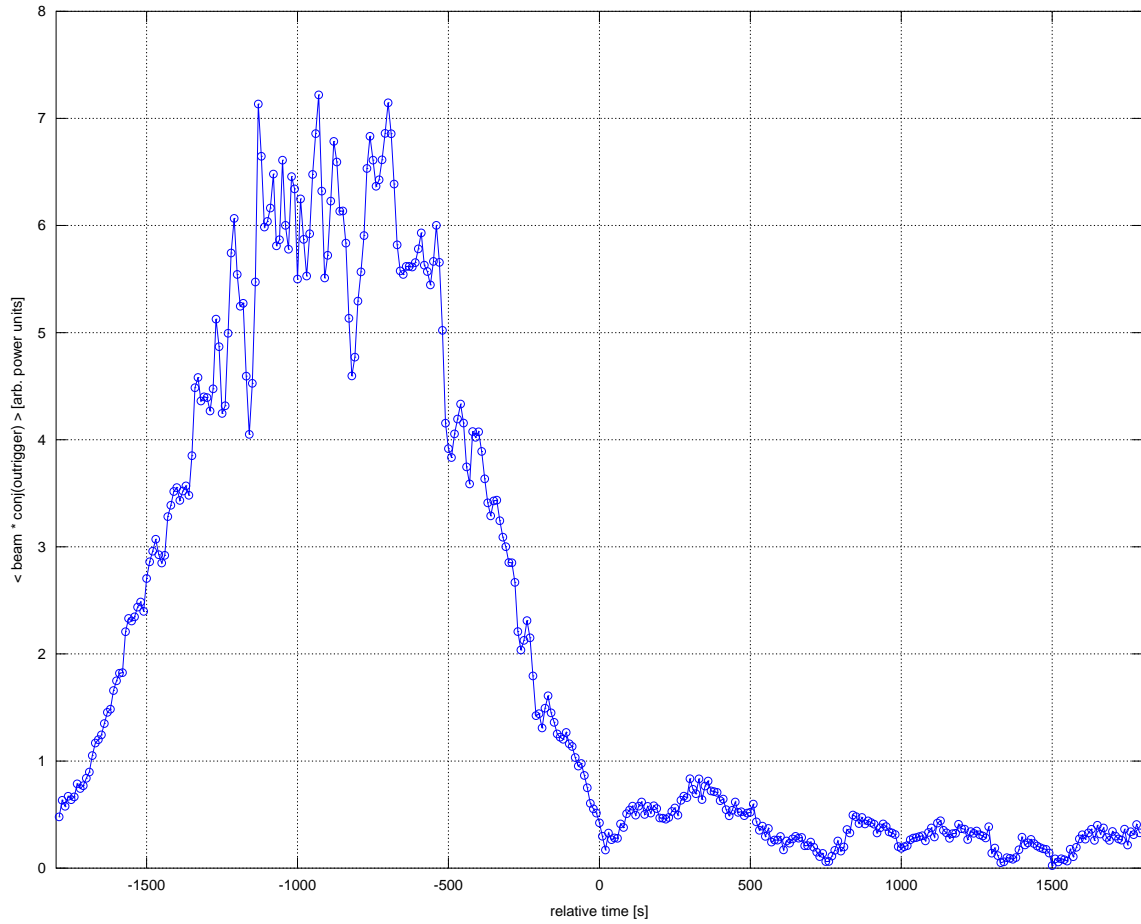
Figure 7: RWR beamforming: Beam repointed to position of Cyg A 15 min (900 s) prior to the midpoint of the dataset, and correlated against the outrigger dipole.
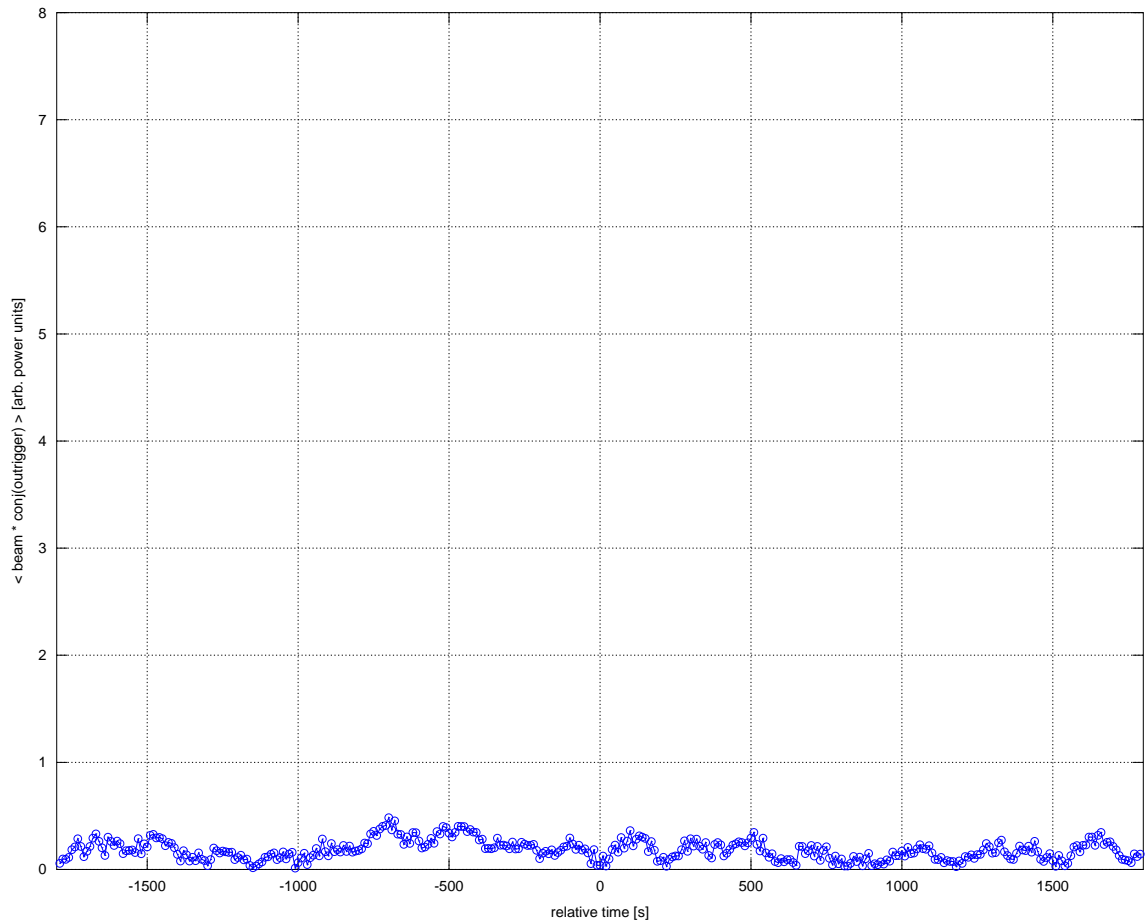
Figure 8: RWR beamforming: Beam repointed to position of Cyg A at the midpoint of the dataset and then shifted 10° toward the horizon (i.e., increasing Z), and correlated against the outrigger dipole. (No detectable source expected.)
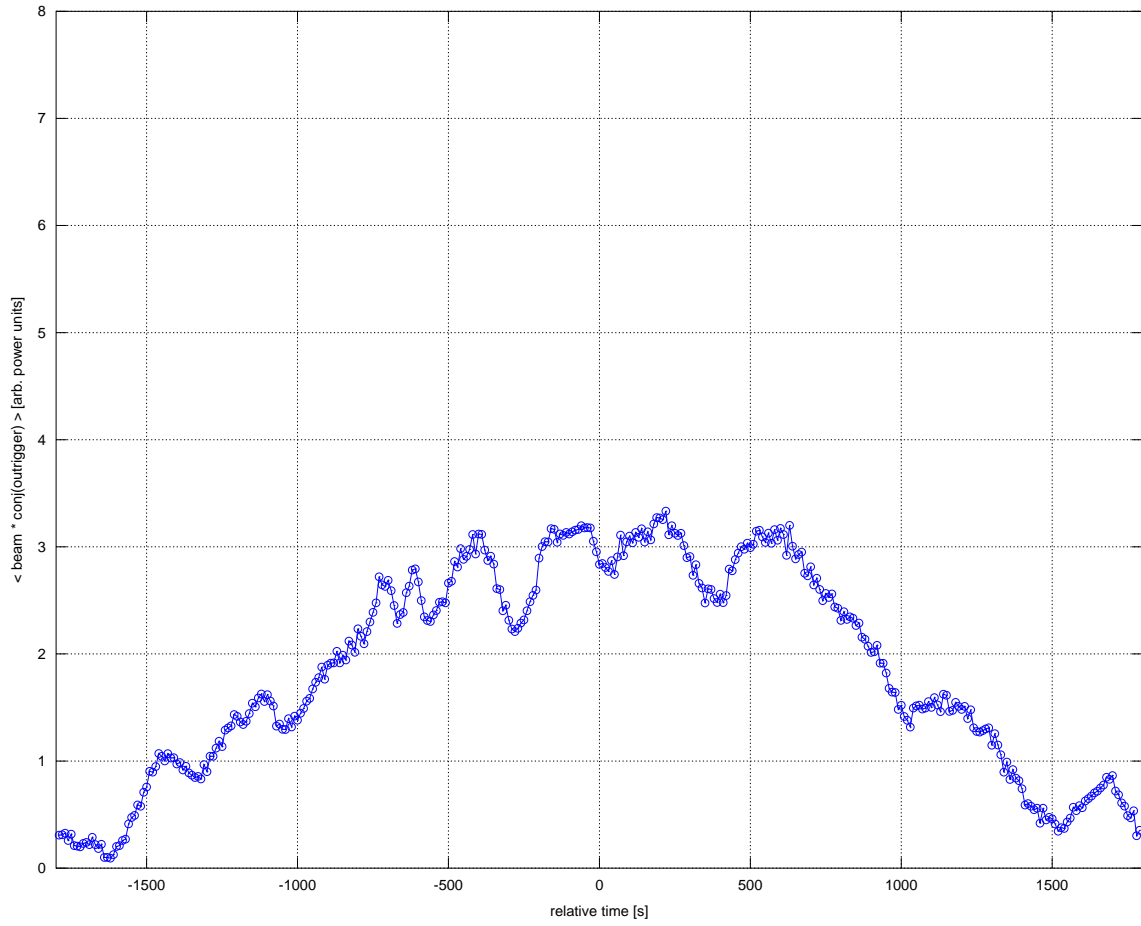
Figure 9: RWR beamforming: Beam repointed to position of Cas A and correlated against the outrigger dipole.

7 Rapid Variation in Fringe Magnitudes – Ionospheric Scintillation?

It is observed in the results of previous sections that large, rapid oscillations on time scales of roughly 10-100 s seem to accompany source detections. Figure 10 shows an attempt to better understand this phenomenon. Each curve is $|\rho_{nm}^{(1)}(t)|$ between some antenna n and the outrigger, filtered to exclude Cas A and the DC contributions. Unlike the procedure described in Section 4, in this case the fringe rate filtering excludes *only* these contributions, leaving behind Cyg A and any higher-frequency content. Since Cyg A then dominates and the antenna patterns are presumably relatively constant over the duration of the observation, the magnitude of the filtered fringes is roughly constant, yet with relatively large, distinctly non-noise-like features. The bottom panel shows the incoherent average of all dipole-outrigger baselines, and seems to indicate some features in common between baselines. Further, comparison of the averaged fringe magnitudes to Figures 4 and 5 seems to suggest the that at least some of the same features exist in the beamformer output. Assuming that it is true that the same variations appear in all baselines as well as the beamformer output, it seems likely that the variations are due to a *bona fide* variation in the source flux, presumably due to ionospheric scintillation. However, additional effort is warranted to confirm that this is the cause, as opposed to some other issue; e.g., long-delay multipath, or an undetected instrumental issue.
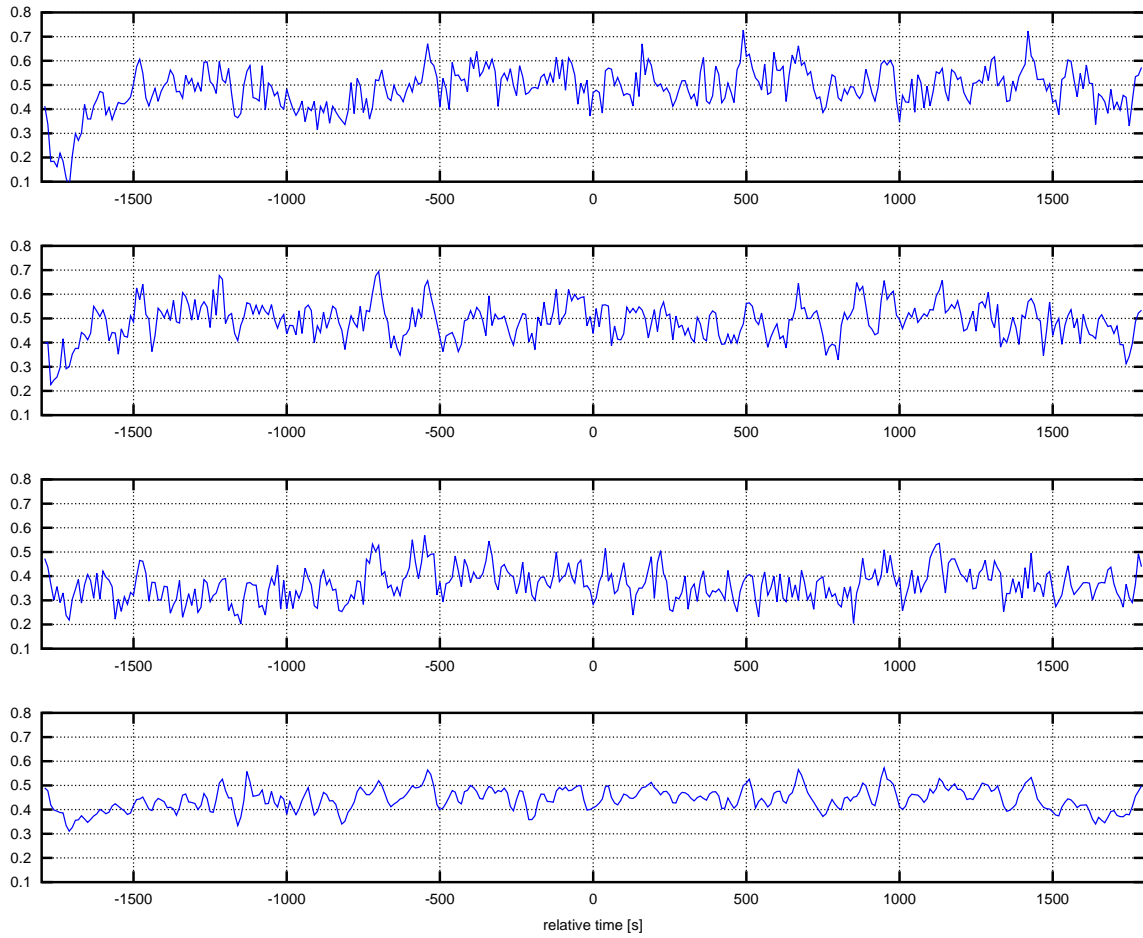
Figure 10: Cyg A fringe magnitudes (filtered to remove Cas A and the DC term). The top three panels are examples from 3 dipole-outrigger baselines; the bottom panel is the incoherent average of all 239 baselines similarly defined.

A Document History

- Version 1 (Sep 13, 2011): First version.

References

[1] J. Hartman, "Antenna pattern measurements from a two-element interferometer," Long Wavelength Array Memo 155, Apr 15, 2009.

[2] J. F. Helmboldt and N. E. Kassim, "The Evolution of Cas A at Low Radio Frequencies," astro-ph/0903.5010, July 7, 2009.

[3] S. W. Ellingson, "Sensitivity of Antenna Arrays for Long-Wavelength Radio Astronomy," *IEEE Trans. Ant. & Prop.*, Vol. 59, No. 6, June 2011, pp. 1855-1863. Also available (preprint form) as LWA Memo 166.

[4] S. Ellingson, "A Parametric Model for the Normalized Power Pattern of a Dipole Antenna over Ground," Long Wavelength Array Memo 175, December 8, 2010.

[5] J. Dowell, "Parametric Model for the LWA-1 Dipole Response as a Function of Frequency," Long Wavelength Array Memo 178, Feb 11, 2011.

[6] L. Kogan & A. Cohen, "A 110 m × 100 m Elliptical Station Design Optimized to Minimize Sidelobes," Long Wavelength Array Memo 150, Jan 8, 2009.